

NON-GAUSSIANITIES IN THE LOCAL CURVATURE OF THE 5-YEAR WMAP DATA

ØYSTEIN RUDJORD^{1,2}, NICOLAAS E. GROENEBOOM^{1,2}, FRODE K. HANSEN^{1,2}, AND PAOLO CABELLA³

(Dated: November 21, 2018)
Draft version November 21, 2018

ABSTRACT

Using the 5 year WMAP data, we re-investigate claims of non-Gaussianities and asymmetries detected in local curvature statistics of the 1 year WMAP data. In Hansen et al 2004, it was found that the northern ecliptic hemisphere was non-Gaussian at the $\sim 1\%$ level testing the densities of hill-, lake and saddle points based on the second derivatives of the CMB temperature map. The 5 year WMAP data has a much lower noise level and better control of systematics. Using these, we find that the anomalies are still present at a consistent level. Also the direction of maximum non-Gaussianity remains. Due to limited availability of computer resources, Hansen et al. 2004 were unable to calculate the full covariance matrix for the χ^2 test used. Here we apply the full covariance matrix instead of the diagonal approximation and find that the non-Gaussianities disappear and there is no preferred non-Gaussian direction. We compare with simulations of weak lensing to see if this may cause the observed non-Gaussianity when using diagonal covariance matrix. We conclude that weak lensing does not produce non-Gaussianity in the local curvature statistics at the scales investigated in this paper. The cause of the non-Gaussian detection in the case of a diagonal matrix remains unclear.

Subject headings: cosmic microwave background — cosmology: observations — methods: statistical

1. INTRODUCTION

During recent years, the investigations of the cosmic microwave background (CMB) has proved to be the most compelling addition to our understanding of the early universe. Observations of the CMB anisotropies, like those obtained by the Wilkinson Microwave Anisotropy Probe (WMAP) experiment (Bennett et al. 2003; Hinshaw et al. 2007), have provided us with profound insight on the composition of structure in our universe. Combined with previous experimental knowledge and a sound theoretical framework, the concordance model of Λ CDM has been established.

The Λ CDM model relies on the framework of inflation. Inflation was initially proposed as a solution to the horizon and flatness problem (Guth et al 1981). Additionally, it established a highly successful scenario for the formation of primordial density perturbations, providing the required seeds for the large-scale structures in the universe. Eventually, these later gave rise to the temperature anisotropies in the cosmic microwave background radiation that we observe today. It is assumed that Gaussian fluctuations in the vacuum field have given rise to these perturbations, so the fluctuations in the CMB map we observe today are also expected to be near Gaussian.

Inflation predicts that the observed universe should be statistically isotropic on large scales. However, during recent years, various anomalies that contradict statistical isotropy have been discovered in the WMAP data (de Oliveira-Costa et al. 2004; Eriksen et al. 2004a; Hansen et al. 2009; Hoftuft et al. 2009; Eriksen et al.

2004b; Hansen et al. 2004; Tegmark et al. 2003; Groeneboom & Eriksen 2009; Groeneboom et al. 2009; Vielva et al. 2004). If these effects are confirmed by the data from the Planck experiment, various anisotropic universe models should be seriously considered.

In order to investigate the properties of different inflationary models, it is important not only to pursue deviations from statistical isotropy, but also any deviations from Gaussianity. Single-field inflation models usually predict a CMB statistically close to Gaussian, but more exotic models may give rise to a larger contribution of non-Gaussianity. In this paper, we focus on a method for testing general deviations from Gaussianity that are not obviously connected to inflationary non-Gaussianity. However, some effort has been made to use the local curvature to estimate the non-Gaussianity parameter f_{NL} (Cabella et al. 2005).

Doré et al. (2003) presented a framework for investigating non-Gaussianities based on the properties of the local curvature of the CMB temperature map. By calculating the second-order derivatives, it is possible to classify each pixel as a “hill”, “lake” or “saddle” based on the eigenvalues of the Hessian matrix. If the map is first smoothed with a Gaussian beam, it is possible to extract the local curvature properties on scales given by the FWHM of the beam. A temperature threshold T_t is introduced, where CMB temperature values below a provided threshold are ignored. Starting with a negative temperature threshold, the fraction of hill, lake and saddle points that have temperatures above the threshold are counted. By performing this analysis on simulated isotropic Gaussian maps, it is possible to estimate what the fraction of hills, lakes and saddle points should be for increasing T_t . This graph is then compared with a similar examination of experimental data using a χ^2 test. It is also possible to predict this plot theoretically, as done by Doré et al. (2003). However, several issues will complicate the task. First, one needs to apply a galaxy mask

oystein.rudjord@astro.uio.no

¹ Institute of Theoretical Astrophysics, University of Oslo, P.O. Box 1029 Blindern, N-0315 Oslo, Norway

² Centre of Mathematics for Applications, University of Oslo, P.O. Box 1053 Blindern, N-0316 Oslo, Norway

³ Dipartimento di Fisica, Università di Roma ‘Tor Vergata’, Via della Ricerca Scientifica 1, I-00133, Roma, Italy

that effectively removes about 20% of the data. There are also point sources to be considered, along with the possibility of excluding large chunks of the sky in order to focus the analysis on specific areas.

Hansen et al. (2004) applied their framework on the 1-yr WMAP data, where no statistical deviation from Gaussianity was found on a full-sky coverage. However, when the authors analyzed independent hemispheres on the CMB sky, they found a non-Gaussian signature on hemispheres centered near the ecliptic poles. The authors therefore suggested that the effect might be due to systematics, and that the direction seems consistent with the results by Eriksen et al. (2004a). However, due to limited computer resources, the authors built their statistics using only 128 and 512 Gaussian simulations, which may be too few for obtaining convergence. For the same reason, they were unable to obtain a full covered covariance matrix for the χ^2 analysis and they therefore ignored the correlations between threshold levels. In addition, the 1-year WMAP data are much more noisy compared to the 5-year data. In this paper, we re-analyze the 5-year WMAP data using an independent and more robust code with a greatly increased number of Gaussian simulations. We also test whether weak lensing may contribute to a non-Gaussian signal in the local curvature statistics.

2. METHOD

The methods in this paper are based on the work done by Hansen et al. (2004) and Doré et al. (2003). We are interested in studying the curvature properties of the temperature fluctuations in the CMB map. Every point on a two-dimensional surface embedded in 3-space can be characterized as being a hill, lake or saddle. In the case of the CMB, we usually express coordinates on \mathbb{S}^2 in spherical coordinates (θ, ϕ) . A hill/lake is where the curvature is negative/positive in both the θ and ϕ directions, whereas a saddle point has negative curvature for one coordinate and positive for the other. While increasing the threshold value T_t , we count the fraction of hill, lake and saddle points for all the pixels with temperature larger than T_t . A simulated CMB map with the classified curvature areas added on top for illustrative purposes is depicted in Figure 1.

2.1. The local curvature

The CMB map is first smoothed with a beam corresponding to the scales that we are interested in. We then normalize the temperature map T with its standard deviation and calculate its various first and second-order covariant derivatives given the spherical coordinates θ and ϕ . That is, we obtain $\frac{dT}{d\theta}$, $\frac{dT}{d\phi}$, $\frac{d^2T}{d\theta^2}$, $\frac{d^2T}{d\phi^2}$ and $\frac{d^2T}{d\theta d\phi}$. For each pixel in the normalized temperature map T , we calculate the Hessian matrix and calculate its eigenvalues λ_1 and λ_2 (as described in Monteserín et al. (2005)). Then, depending on the sign of the eigenvalues, we classify every point on the sphere as a hill ($\lambda_1 > 0, \lambda_2 > 0$), lake ($\lambda_1 < 0, \lambda_2 < 0$) or saddle point ($\lambda_1, \lambda_2 < 0$).

By performing this analysis on simulated isotropic Gaussian maps, it is possible to estimate what the mean fraction of hills, lakes and saddle points should be for increasing T_t , together with the standard deviation. An example of such a graph is presented in Figure 2.

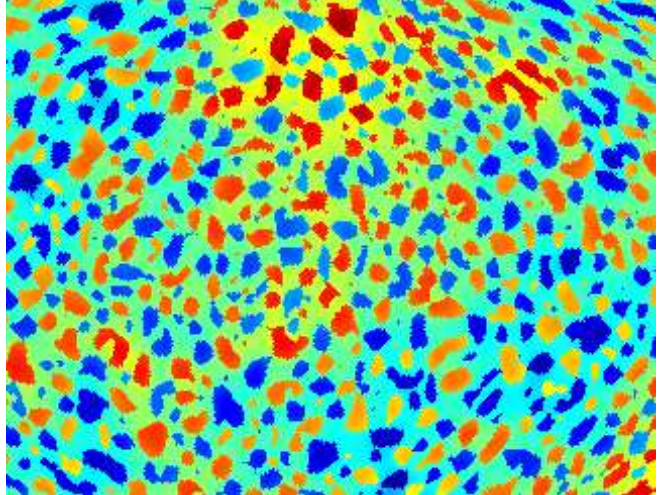


FIG. 1.— The classification of hills (red parts), lakes (blue parts) and saddles (neutral, in between). The original CMB map is added in the background for illustrative purposes. The beam FWHM used in this example is 500' on an isotropic realization of the best-fit Λ CDM power spectrum.

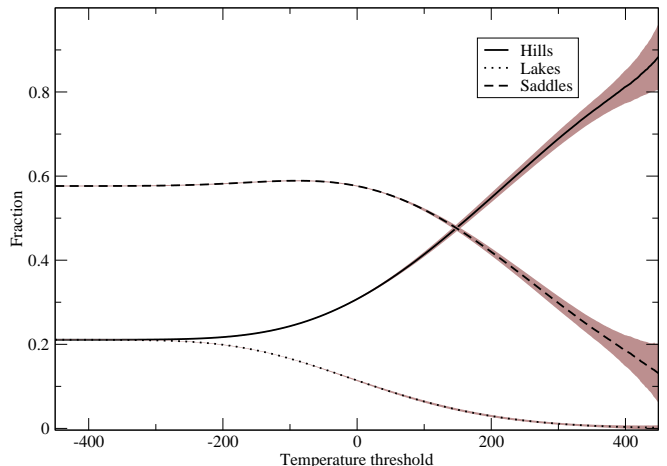


FIG. 2.— The fraction of hills, lakes and saddle pixels in a simulated Gaussian map with $n_{\text{side}} = 512$. The simulation is generated from the best-fit powerspectrum from the WMAP 5 year release. The black line depicts the mean, while the shaded area is the 68% confidence area.

2.2. The extended mask

When working with experimental CMB data, we need to remove a portion of the sky due to foreground residuals. In this paper, we operate with several masks, most notably the WMAP KQ85 sky cut (Gold et al. 2008), which removes 18% of the sky. The edges of the mask need special consideration, due to the differentiation of the map. We therefore perform the following procedure for generating suitable CMB masks:

1. Start with the 5-year WMAP KQ85 or KQ75 mask without point source holes.
2. The mask is expanded by b° , where b is the smoothing angle FWHM to avoid effects of the smoothed mask. Note that this step was not used in Hansen et al. (2004). We thus use an extended mask which is considerably much larger than the one used in Hansen et al. (2004). As pointed out

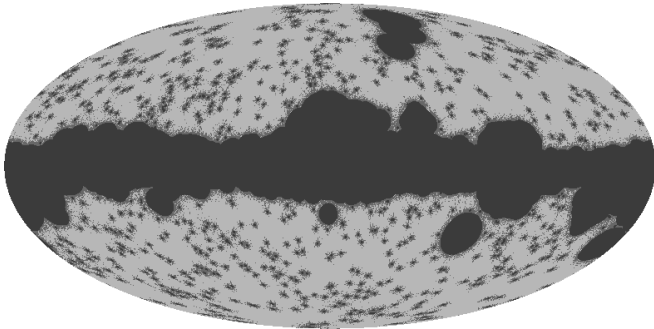


FIG. 3.— The KQ85 mask expanded with 5° and point-sources added. The expansion from differentiation is indicated in grey.

- below, we have compared results also with the smaller extended mask for which this step was omitted.
- Point source holes are added to the mask after expansion. If added before smoothing, the smeared point sources would nearly fill the mask.
 - The mask is differentiated, and then normalized. By normalized, we mean that each pixel p_i is set to $p_i = \frac{|p_i|}{p_{max}}$.
 - If a pixel in a normalized, differentiated map has value above a certain threshold, the pixel is masked out. We have used the threshold 0.02 throughout this paper.

2.3. χ^2 statistics

We now present a method for estimating how much a CMB data set deviates from Gaussianity, based on standard statistical tests. We calculate the covariance matrix \mathbf{C} from the fraction of hills, lakes and saddles for 40000 Gaussian simulations. We implement a standard χ^2 -test on the form

$$\chi^2 = \mathbf{d}^T \mathbf{C}^{-1} \mathbf{d}, \quad (1)$$

where $\mathbf{d} = X_{T_t} - \langle X \rangle_{T_t}$ and X_{T_t} is a hill, lake or saddle density at threshold T_t . We then estimate the χ^2 on 10000 simulations, and obtain a histogram of the distribution, as presented in Figure 4. When performing the analysis on WMAP data, we first calculate the χ^2 and then compare it to the pre-calculated χ^2 distribution. We then count the percentage of the χ^2 s that are above the experimental, i.e. if 32% of the simulated χ^2 values are larger than the χ^2 from experimental data this corresponds to 1σ deviation from the Gaussian expectation. A value of 5% would be consistent with a 2σ deviation from the Gaussianity.

As an alternative method we also use a diagonal covariance matrix for calculating the χ^2 values, thus ignoring correlations between threshold levels. This is the method applied in Hansen et al. (2004).

3. DATA

We consider the publicly available 5-year WMAP data (Bennett et al. 2003; Hinshaw et al. 2007) that can be obtained from the LAMBDA⁴ site. We primarily perform the analyses on a combined V and W frequency

⁴ <http://lambda.gsfc.nasa.gov/>

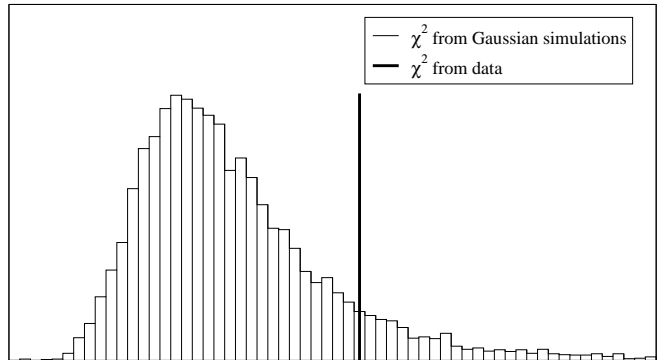


FIG. 4.— An example of a table with χ^2 obtained from Gaussian simulations (histogram) and a χ^2 from real data (line). The fraction of simulated χ^2 above the χ^2 from real data describes its deviation from the Gaussian mean.

band (94 and 61 GHz) in order to keep noise and foregrounds to a minimum. In addition to the 5-yr WMAP data, we also simulate 50000 Gaussian CMB maps based on the best-fit angular powerspectrum from the 5-year WMAP release. We convolve the simulated maps with the combined V and W instrumental beam before adding Gaussian noise. All CMB maps considered in this paper have Healpix resolution $N_{\text{side}} = 512$.

We focus on several different divisions of the sky. First, we consider the full-sky WMAP data including the extended KQ85 and the KQ75 mask from Section 2.2. We then investigate the northern and southern galactic hemispheres individually, using only the KQ85 mask. Due to the alignment of the WMAP satellite with the ecliptic plane, we also include an analysis of the northern and southern ecliptic hemispheres. We then perform the full-sky analysis on a co-added Q-band data set, a co-added V-band set and a co-added W-band set. Finally, we re-analyze the co-added V+W data sets on hemispheres centered around all the pixel centers on a map with $N_{\text{side}} = 2$. From these results, we obtain maps with preferred directions depicting the amount of deviation from Gaussianity on the sky.

4. RESULTS

Here we present the results, first with a full covariance matrix and then without.

4.1. Results with full covariance matrix

The results from the V+W full sky and north/south galactic/ecliptic analyses are presented in Table 1. The most interesting result from Table 1 is the $\sim 1\%$ deviation from Gaussianity in the full-sky at 3° when counting saddles. A general trait throughout the analysis is that scales above and below 3° have deviation from Gaussianity no more than 2σ . We continue by analyzing whether the 1% detection on the full-sky can be observed in the various WMAP frequency bands alone. We therefore perform the same full-sky analysis on the Q, V and W frequency bands. The results are shown in Table 3, and are consistent with the combined V+W full-sky analysis, where a 2σ deviation from Gaussianity is visible in all band for saddles at 3° .

Motivated by the asymmetry found in Hansen et al. (2004), we perform the analysis on all hemispheres centered around pixels on a map with $N_{\text{side}} = 2$ using the

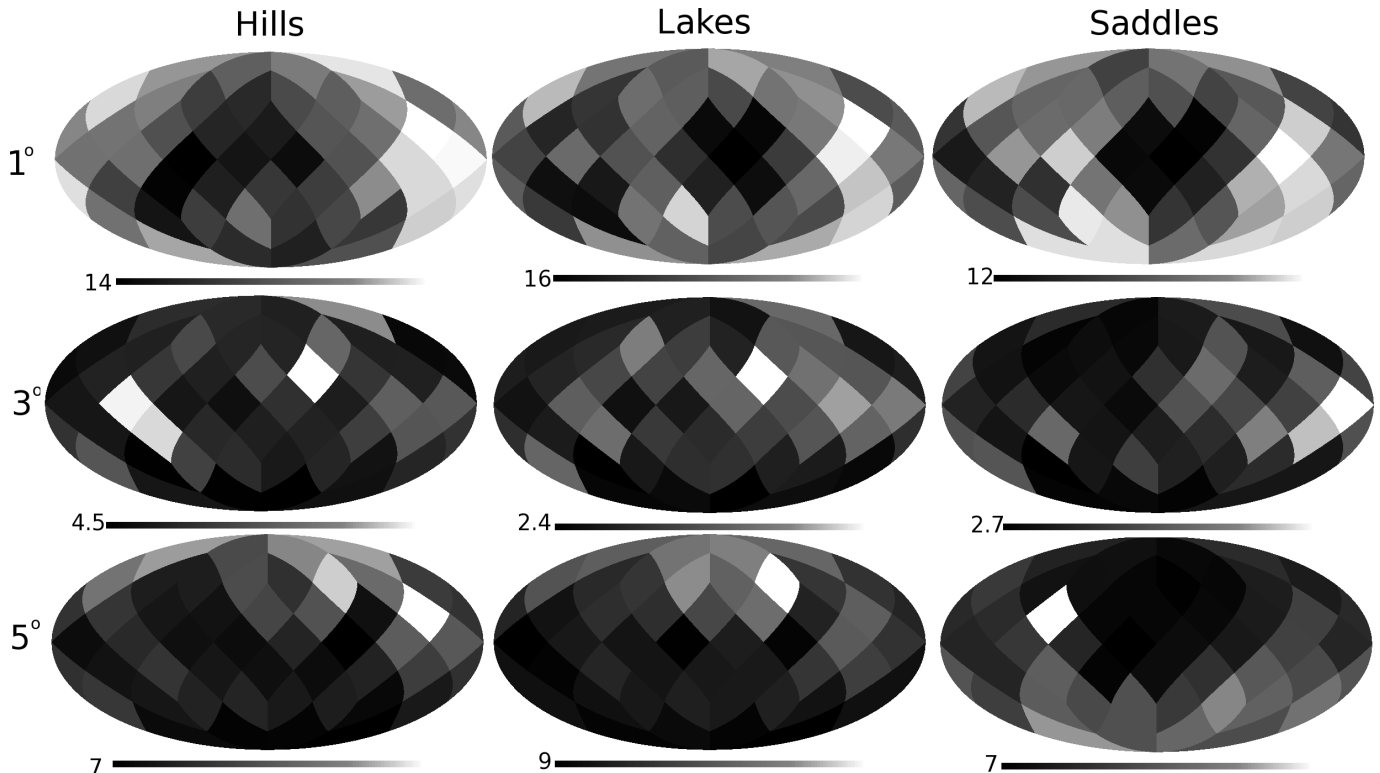


FIG. 5.— The results from a non-Gaussian analysis of hemispheres centered around pixels on a map with $N_{\text{side}} = 2$. Darker pixels correspond to higher deviations from Gaussianity on a hemisphere centered around this pixel. The values of the pixels indicate the percentage of simulations with a higher χ^2 . Whiter pixels correspond to $< 1\sigma$ levels.

co-added V+W data set. This analysis used the extended KQ85 mask. The results are shown in Figure 5, where darker pixels represent larger deviations from Gaussianity on a hemisphere centered around the pixel. Here, whiter pixels correspond to $< 1\sigma$ levels. These results agree with the full-sky analysis and with the ecliptic/galactic hemispherical analyses, and show that there is no apparent preferred direction in either of the data sets.

Finally, we perform a χ^2 test of the combined results. We construct a data vector containing all fractions of hills and lakes for all thresholds and smoothing scales (1° , 3° and 5°). The covariance matrix including all correlations between hills and lakes and between different scales, is calculated from Gaussian simulations. We estimate a χ^2 value for both WMAP data and simulations. The final comparison shows that 80% of the simulations have a higher χ^2 value than the simulations for the combined V + W channel. In other words, when using the full covariance matrix, there is full consistency with the Gaussian hypothesis.

4.2. Comparison with earlier work

Hansen et al. (2004) found very little evidence for deviation from Gaussianity in the 1-year WMAP data when analyzing full-sky CMB maps using the Kp2 galaxy mask. This is in good agreement with the findings in this paper, where we have shown there is at most a 2σ deviation from Gaussianity in the saddles at 3° in the combined V+W data. We stress that while the number of simulated Gaussian maps used for the χ^2 test by Hansen et al. (2004) was 512, we have used 50 000. Where Hansen et al. (2004) employed a covariance ma-

trix that was strictly diagonal, we have operated with a full covariance matrix including correlations between different thresholds. In addition, the 1-year WMAP data are in general more contaminated by instrumental noise than the 5-year data.

When using the full covariance matrix, the directional analysis show that there isn't any preferred direction for deviations from Gaussianity. Figure 5 shows that the directions for various scales seem to be randomly scattered, and the significance is very low. In fact, only at 3° there seems to be a 2σ hint, but any exact directions are non-existent. This is in disagreement with the results from Hansen et al. (2004), who claimed that there exists a maximum of non-Gaussianity on hemispheres centered at the ecliptic poles.

However, when we ignore correlations and use a strictly diagonal covariance matrix, the results are more in agreement with Hansen et al. (2004). These results are presented in Table 2, where we note several deviations at the less than 1% level. Also, when performing the directional analysis, we find that the non-Gaussian signal has a clear maximum close to (but not directly on) the ecliptic north-pole, as seen in figure 6 and Table 2. This is in agreement with the direction described by Hansen et al. (2004). As noted above, here we use a larger extended mask than in Hansen et al. (2004). We have also tested with the smaller extended mask and find results similar to the ones presented in Table 2. We conclude that by using a diagonal approximation to the correlation matrix, we still find non-Gaussianities and asymmetries over several scales and with different masks, including the full covariance matrix lowers the effect of the non-Gaussian signatures and the hemispherical anisotropy.

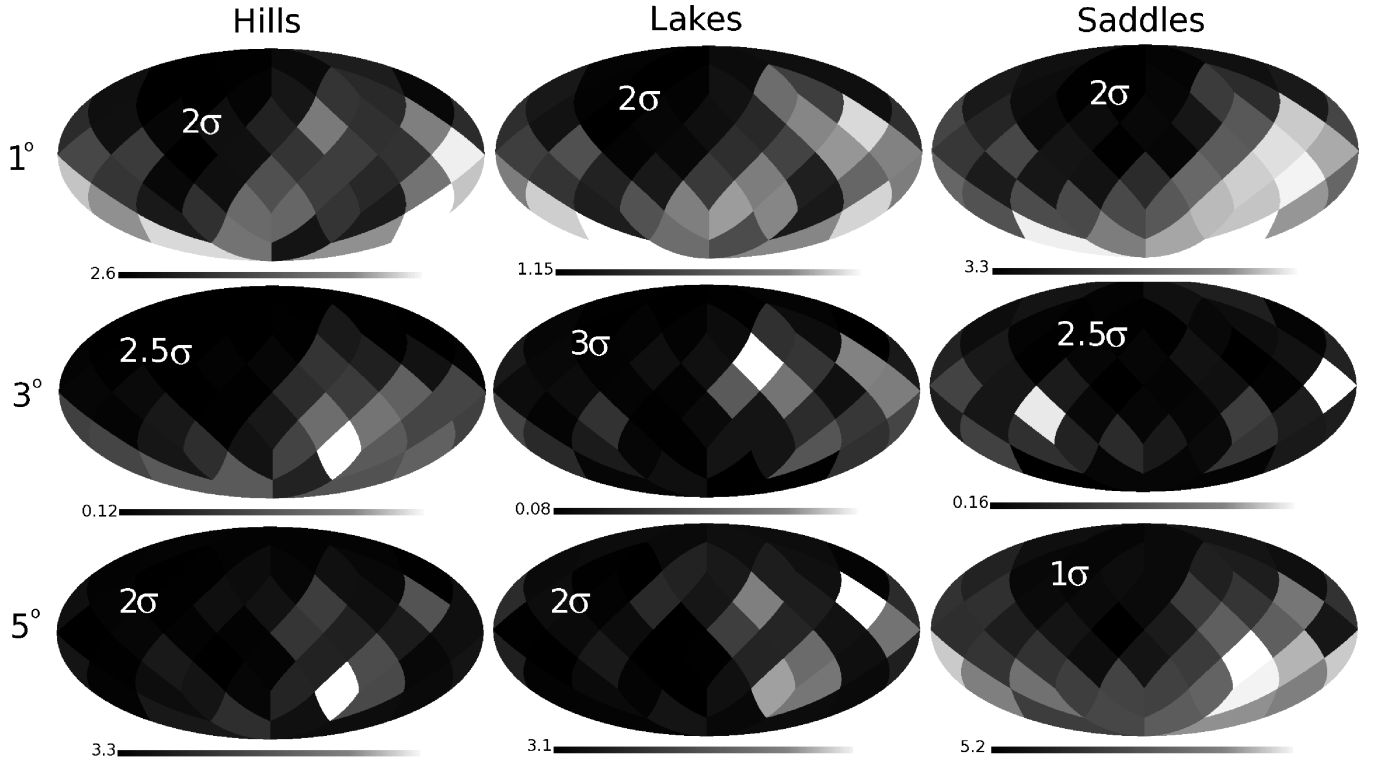


FIG. 6.— The results from a non-Gaussian analysis using a diagonal covariance matrix, of hemispheres centered around pixels on a map with $N_{\text{side}} = 2$. Darker pixels correspond to higher deviations from Gaussianity on a hemisphere centered around this pixel. The values of the pixels indicate the percentage of simulations with a higher χ^2 . Whiter pixels correspond to $< 1\sigma$ levels.

4.3. Tests on weak lensing simulations

In order to investigate whether the deviations may be a result of weak lensing in the CMB, we performed another test. We used the freely available `LensPix`⁵ code (Lewis (2005)) to simulate 300 Gaussian CMB maps, and 300 CMB maps with weak lensing. For the simulations we used the best-fit power spectrum and lensing potential provided by the WMAP team. The procedure of counting hills, lakes and saddles as described above was applied to all the simulations. From the Gaussian simulations we found mean values and standard deviations of hill, lake and saddle fractions at different smoothing scales. We then compared these with the results from the simulations with weak lensing. We found no significant deviation in the local curvature of the simulations with lensing. We therefore conclude that the deviations from non-Gaussianity described in this paper and Hansen et al. (2004) are not caused by weak lensing in the CMB.

5. CONCLUSIONS

We have developed an independent framework for estimating deviations from Gaussianity in CMB data based on the methods established by Doré et al. (2003) and Hansen et al. (2004). The methods used are model-independent, and do not share any obvious connections with non-Gaussianity frameworks of known physical origin. By counting the fraction of lakes, hills and saddles in simulated Gaussian maps while increasing the temperature threshold, we have built a distribution for what is expected for Gaussian maps. We then compared ex-

perimental data to this distribution, determining the deviation from the Gaussian assumption. We then considered a combined V + W full-sky data set with the extended KQ85 and KQ75 mask, and found evidence of a $\sim 1\%$ deviation from Gaussianity on scales around 3° . We also analyzed other scales as well as the north and south galactic/ecliptic hemispheres separately, but discovered no deviation from Gaussianity greater than 2σ . We continued by performing an analysis on each of the hemispheres centered around a pixel on a Healpix map with $N_{\text{side}} = 2$ using the combined V+W data. We produced directional maps for hills, lakes, saddles using the three scales, and found no evidence for a preferred direction in either of the maps. Finally, we calculated the combined χ^2 from all our results, which resulted in an overall agreement with Gaussianity. We conclude that there is no significant evidence for non-Gaussianities or asymmetries in the WMAP data based on this test.

However, in Hansen et al. (2004), it was found that the northern ecliptic hemisphere was non-Gaussian based on similar local curvature measurements. There was however one large difference in the method used: In that work, a diagonal approximation to the covariance matrix was applied. Repeating our analysis with a diagonal covariance matrix we obtain similar results as Hansen et al. (2004). Taking into account correlations between thresholds, the non-Gaussianity disappears. We have compared Gaussian CMB simulations to CMB simulations with weak lensing to see whether the hill, lake or saddle densities are different in the two sets of simulations. No significant differences were found. We therefore conclude that weak lensing may not cause the non-gaussianity found when using a diagonal correlation matrix. It is still un-

⁵ <http://cosmologist.info/lenspix/>

TABLE 1
SUMMARY OF DEVIATIONS FROM GAUSSIANTY IN THE COMBINED
V+W DATA

Area/Scale	60'	180'	300'
Full sky + KQ85 mask			
hills	27%	6.7%	3.87%
saddles	69%	1.13%	11%
lakes	46%	15%	6.5%
Full sky + KQ75 mask			
hills	48%	10%	14%
saddles	85%	1.33%	7%
lakes	92%	14%	16%
Northern galactic hemisphere			
hills	86%	30%	46%
saddles	75%	13%	25%
lakes	73%	18%	38%
Southern galactic hemisphere			
hills	39%	5%	10%
saddles	78%	5%	54%
lakes	53%	5%	12%
Northern ecliptic hemisphere			
hills	64%	28%	15%
saddles	83%	5%	20%
lakes	69%	45%	25%
Southern ecliptic hemisphere			
hills	73%	13%	13%
saddles	75%	15%	54%
lakes	62%	14%	17%

NOTE. — The values correspond to the fraction of χ^2 from isotropic simulations that have a higher χ^2 than the analysis of the data set. A low percentage would thus indicate a non-Gaussianity.

TABLE 2
SUMMARY OF DEVIATIONS FROM GAUSSIANTY IN THE COMBINED
V+W DATA USING A STRICTLY DIAGONAL COVARIANCE MATRIX

Area/Scale	60'	180'	300'
Full sky + KQ85 mask			
hills	12%	0.95%	0.68%
saddles	11%	0.034%	10%
lakes	11%	0.67%	0.64%
Northern ecliptic hemisphere			
hills	13%	0.38%	4.2%
saddles	11%	0.34%	11%
lakes	3.8%	0.67%	4.2%
Southern ecliptic hemisphere			
hills	39%	30%	15%
saddles	78%	4.0%	87%
lakes	29%	3.4%	12%

NOTE. — The values correspond to the fraction of χ^2 from isotropic simulations that have a higher χ^2 than the analysis of the data set. A low percentage would thus indicate a non-Gaussianity.

TABLE 3
SUMMARY OF DEVIATIONS FROM GAUSSIANTY IN FULL-SKY
COMBINED BANDS

Area/Scale	60'	180'	300'
Full-sky combined W-band			
hills	20%	7.5%	5.9%
saddles	66%	2.8%	24%
lakes	37%	27%	5%
Full-sky combined V-band			
hills	24%	11%	8.2%
saddles	39%	1.61%	13%
lakes	65%	27%	7%
Full-sky combined Q-band			
hills	15%	6.6%	3.13%
saddles	76%	1.73%	8.9%
lakes	34%	25%	5%

NOTE. — The values correspond to the fraction of χ^2 from isotropic simulations that have a higher χ^2 than the analysis of the data set. A low percentage would thus indicate a non-Gaussianity.

clear what causes the detection of non-Gaussianity when a diagonal correlation matrix is used. Even though the χ^2 test is not optimal when correlations are ignored, we are still comparing the data to simulations for which an identical procedure (i.e. diagonal approximation to the covariance matrix) has been applied. If the best fit model estimated from the data is correct, one would expect simulations based on this model to have the same statistical properties as the data, no matter which statistical test is performed. There is thus still a discrepancy between data and simulations based on the model which best fits the data. Whether this discrepancy is a statistical fluke or may arise from systematic errors/cosmology and whether it is related to other asymmetries is still unclear.

FKH and NEG acknowledge support from the research council of Norway. We acknowledge use of the HEALPix⁶ software (Górski et al. 2005) and analysis package for deriving the results in this paper. We acknowledge the use of the Legacy Archive for Microwave Background Data Analysis (LAMBDA). Support for LAMBDA is provided by the NASA Office of Space Science.

⁶ <http://healpix.jpl.nasa.gov>

REFERENCES

- Bennett, C. L., et al. 2003, *ApJS*, 148, 1
- Cabella, P., Liguori, M., Hansen, F. K., Marinucci, D., Matarrese, S., Moscardini, L., Vittorio, N. 2005, *MNRAS*, 358, 684
- de Oliveira-Costa, A., Tegmark, M., Zaldarriaga, M., & Hamilton, A. 2004, *Phys. Rev. D*, 69, 063516
- Doré, O., Colombi, S., & Bouchet, F. R. 2003, *MNRAS*, 344, 905
- Eriksen, H. K., Hansen, F. K., Banday, A. J., Górski, K. M., & Lilje, P. B. 2004a, *ApJ*, 609, 1198
- Eriksen, H. K., Hansen, F. K., Banday, A. J., Górski, K. M. & Lilje, P. B. 2004, *ApJ*, 605, 14
- Gold, B., et al. 2008, *ApJ*, submitted, [arXiv:0803.0715]
- Górski, K. M., Hivon, E., Banday, A. J., Wandelt, B. D., Hansen, F. K., Reinecke, M., & Bartelmann, M. 2005, *ApJ*, 622, 759
- Guth, A. H, 1981, *Phys. Rev. D*, 347
- Groeneboom, N. E., & Eriksen, H. K. 2009, *ApJ*, 690, 1807
- Groeneboom, N. E., Eriksen, H. K., Gorski, K., Huey, G., Jewell, J., & Wandelt, B. 2009, *ApJ*, 702, L87
- Hansen, F. K., Banday, A. J., & Górski, K. M. 2004, *MNRAS*, 354, 641
- Hansen, F. K., Cabella, P., Marinucci, D. & Vittorio, N. 2004, *ApJ*, 607, L67
- Hansen, F. K., Banday, A. J., Górski, K. M., Eriksen, H. K., & Lilje, P. B. 2009, *ApJ*, 704, 1448
- Hinshaw, G., et al. 2007, *ApJS*, 170, 288
- Hoftuft, J. et al. 2009, in press, arXiv:0903.1229
- Lewis, A. 2005, *Phys. Rev. D*, 71, 083008
- Monteserín, C., Barreiro, R. B., Sanz, J. L., & Martínez-González, E. 2005, *MNRAS*, 360, 9
- Tegmark, M., de Oliveira-Costa, A. & Hamilton, A. J. 2003, *Phys. Rev. D*, 68, 123523
- Vielva, P., Martínez-González, E., Barreiro, R. B., Sanz, J. L., & Cayón, L. 2004, *ApJ*, 609, 22